

# Supernova constraints on Multi-coupled Dark Energy

Arpine Piloyan,<sup>1</sup> Valerio Marra,<sup>2</sup> Marco Baldi,<sup>3,4</sup> and Luca Amendola<sup>2</sup>

<sup>1</sup>*Yerevan State University, Alex Manoogian 1, Yerevan 0025, Armenia*

<sup>2</sup>*Institut für Theoretische Physik, Universität Heidelberg, Philosophenweg 16, 69120 Heidelberg, Germany*

<sup>3</sup>*Dipartimento di Fisica e Astronomia, Università di Bologna, Viale C. Berti-Pichat 6/2, I-40127, Bologna*

<sup>4</sup>*INAF, Osservatorio Astronomico di Bologna, Viale C. Berti-Pichat 6/2, I40127, Bologna*

The persisting consistency of ever more accurate observational data with the predictions of the standard  $\Lambda$ CDM cosmological model puts severe constraints on possible alternative scenarios, but still does not shed any light on the fundamental nature of the cosmic dark sector. As large deviations from a  $\Lambda$ CDM cosmology are ruled out by data, the path to detect possible features of alternative models goes necessarily through the definition of cosmological scenarios that leave almost unaffected the background and – to a lesser extent – the linear perturbations evolution of the universe. In this context, the Multi-coupled DE (McDE) model was proposed by Baldi [9] as a particular realization of an interacting Dark Energy field characterized by an effective screening mechanism capable of suppressing the effects of the coupling at the background and linear perturbation level. In the present paper, for the first time, we challenge the McDE scenario through a direct comparison with real data, in particular with the luminosity distance of Type Ia supernovae. By studying the existence and stability conditions of the critical points of the associated background dynamical system, we select only the cosmologically consistent solutions, and confront their background expansion history with data. Confirming previous qualitative results, the McDE scenario appears to be fully consistent with the adopted sample of Type Ia supernovae, even for coupling values corresponding to an associated scalar fifth-force about four orders of magnitude stronger than standard gravity. Our analysis demonstrates the effectiveness of the McDE background screening, and shows some new non-trivial asymptotic solutions for the future evolution of the universe. Clearly, linear perturbation data and, even more, nonlinear structure formation properties are expected to put much tighter constraints on the allowed coupling range. Nonetheless, our results show how the background expansion history might be highly insensitive to the fundamental nature and to the internal complexity of the dark sector.

PACS numbers: 98.80.-k, 04.40.-b, 95.36.+x, 95.35.+d, 97.60.Bw, 98.80.Es.

Keywords: dark energy theory, dark matter theory, supernova type Ia - standard candles, dark energy experiments

## I. INTRODUCTION

The standard model of cosmology – characterized by the existence of two distinct forms of gravitating energy that do not interact with the electromagnetic field, thereby evading direct observations – has been tremendously challenged over the past decade by the impressive improvements in the accuracy of observational tests. Despite the wide variety of complementary probes that have been progressively developed in order to test the consistency of the model, covering a huge range of scales and redshifts, no significant deviation from the predictions of standard cosmology has been detected so far, even with the exquisite accuracy recently reached by the Planck satellite [2]. Nonetheless, such ever-increasing accuracy in the consistency checks on the model and in the precise determination of its few basic parameters has shed no light on the fundamental nature of the two dominating constituents of the Universe, Dark Energy (DE) and Cold Dark Matter (CDM).

While the former appears to be fully consistent with the predictions of a cosmological constant  $\Lambda$ , more sophisticated possibilities like dynamical or interacting DE, or large-scale modifications of gravity (see e.g. [6]), have not yet been excluded, and retain most of their original ap-

peal as possibly alleviating the fundamental fine-tuning problems of  $\Lambda$ . In particular, several alternative DE scenarios can mimic the evolution of a cosmological constant closely enough to evade present observational bounds. Similarly, while the evidence in favor of a CDM component from astrophysical and cosmological observations is now hardly controvertible, none of the experimental efforts put in place so far have been able to provide a clear and statistically significant detection of any of the plausible CDM particle candidates, arising in different extensions of the standard model of particle physics.

In such context, it is interesting to explore speculative models with a higher level of internal complexity of either of these two mysterious dark fields, or possibly of both, as long as present observational bounds are matched. In particular, for what concerns the DE sector, dynamical DE models such as *Quintessence* [31, 36] or *k-essence* [7] have been proposed, possibly also featuring non-negligible perturbations at sub-horizon scales [12, 17, 18, 33] or direct interactions with CDM [3, 8, 19, 37] or massive neutrinos [4], as well as modified gravity models [21]. While a large portion of the parameter space of such models has been progressively ruled out by increasingly accurate observational constraints, the range of parameters that remains viable still offers the chance of some relevant non-standard phe-

nomenology [see e.g. 30]. Similarly, for the CDM sector, several possible extensions of the standard model have been proposed, ranging from Warm Dark Matter models [WDM, see e.g. 15] to Self-Interacting Dark Matter [SIDM, see e.g. 1, 20, 25, 35] or mixed Cold+Warm Dark Matter scenarios [22, 27], characterized by the existence of more than one Dark Matter particle species. More recently, models with almost degenerate multiple CDM species have been also considered [see 28].

While the most basic and widely investigated models of interactions between the DE field and CDM particles are now robustly constrained through their predicted impact on the background and linear perturbation evolution [see e.g. 13, 23, 29, 32, 38] as well as through their effects on nonlinear structure formation [8, 11, 24, 26], Brookfield et al. [16] have recently shown that if DE interactions are associated with a higher level of complexity of the CDM sector, such constraints might significantly relax, leaving room for a new class of non-standard cosmological scenarios. More specifically, if DE interacts with different couplings to different species of CDM particles, the impact of the interaction on background and linear perturbations can be relatively mild even for individual coupling values largely exceeding the present observational bounds for the case of an interaction with a single CDM species.

While the drawback of such class of models might reside in the need to introduce a large number of new free parameters associated with each individual interaction channel, we will focus in the present paper on a particular realization of this scenario recently proposed by Baldi [9], which involves only two different species of CDM particles characterized by the same absolute value of the coupling to the DE field but with opposite signs, thereby requiring no more parameters than a standard interacting DE model.

In the present paper, we will provide the first direct comparison of such a ‘‘Multi-coupled DE’’ (McDE) scenario with the supernova luminosities of the publicly available Union2.1 sample [34]. Confirming previous qualitative results, our analysis will show how present observational data on the background expansion are fully consistent with McDE scenarios even for very large values of the DE coupling, up to three orders of magnitude larger than present bounds on the coupling for standard cDE models.

The present work is organized as follows. In section II we will review the main background equations characterizing the McDE scenario; in section III we will perform a phase-space analysis of the critical points of the system, discussing their existence and stability conditions; in section IV we will introduce the data sample adopted in our analysis and the methods employed to compare data with the McDE expectations, and in section V we will discuss the outcomes of such comparison. Finally, in section VI we will draw our conclusions.

## II. BACKGROUND EQUATIONS

As mentioned above, we will study the model proposed in the Ref. [9], defined by the action integral

$$S = \int d^4x \sqrt{-g} \left[ \frac{M_{Pl}^2}{2} R + \frac{1}{2} \dot{\phi}^2 - \sum_{\pm} m_{\pm} e^{\pm C\phi} \bar{\psi}_{\pm} \psi_{\pm} - V(\phi) + \mathcal{L}_r \right], \quad (1)$$

where  $g$  is the determinant of the metric tensor,  $M_{Pl} = 1/\sqrt{8\pi G}$  is the reduced Planck mass and  $\mathcal{L}_r$  is the Lagrangian of the relativistic components. The new idea of the model is the introduction of two different CDM species  $\psi_{\pm}$  interacting with the scalar field  $\phi$  through the dimensional couplings  $\pm C$ . For simplicity, we will not consider the baryonic component of the Universe in this work. In a homogeneous and isotropic Friedmann-Lemaître-Robertson-Walker (FLRW) model with scale factor  $a$  and no spatial curvature, the field equations of McDE cosmologies are as follows:

$$\ddot{\phi} + 3H\dot{\phi} + \frac{dV}{d\phi} = +C\rho_- - C\rho_+, \quad (2)$$

$$\dot{\rho}_- + 3H\rho_- = -C\dot{\phi}\rho_-, \quad (3)$$

$$\dot{\rho}_+ + 3H\rho_+ = C\dot{\phi}\rho_+, \quad (4)$$

$$\dot{\rho}_r + 4H\rho_r = 0, \quad (5)$$

$$3M_{Pl}^2 H^2 = \rho_r + \rho_+ + \rho_- + \rho_{\phi}, \quad (6)$$

where an overdot represents a derivative with respect to the cosmic time  $t$ ,  $H \equiv \dot{a}/a$  is the Hubble function, and the total CDM density is related to the two dark matter densities  $\rho_{\pm}$  by  $\rho_{CDM} = \rho_+ + \rho_-$ . As in Ref. [9] we introduce the asymmetry parameter  $\mu$  as follows:

$$\mu = \frac{\Omega_+ - \Omega_-}{\Omega_+ + \Omega_-}, \quad (7)$$

where the fractional density parameters  $\Omega_i$  are given by

$$\Omega_i = \frac{\rho_i}{3H^2 M_{Pl}^2}. \quad (8)$$

We will denote with a subscript ‘‘0’’ and ‘‘in’’, respectively, present-day and initial values of time-dependent parameters such as  $\mu$ . We also introduce a dimensionless coupling constant  $\beta$  defined as:

$$\beta \equiv \sqrt{\frac{3}{2}} M_{Pl} C. \quad (9)$$

Following Ref. [9], we restrict our analysis to the case of an exponential self-interaction potential of the form:

$$V(\phi) = V_0 e^{-\alpha_1 \phi} \quad (10)$$

This particular choice simplifies the equations in analogy with the single-field coupled dark energy model of Refs [3, 37].

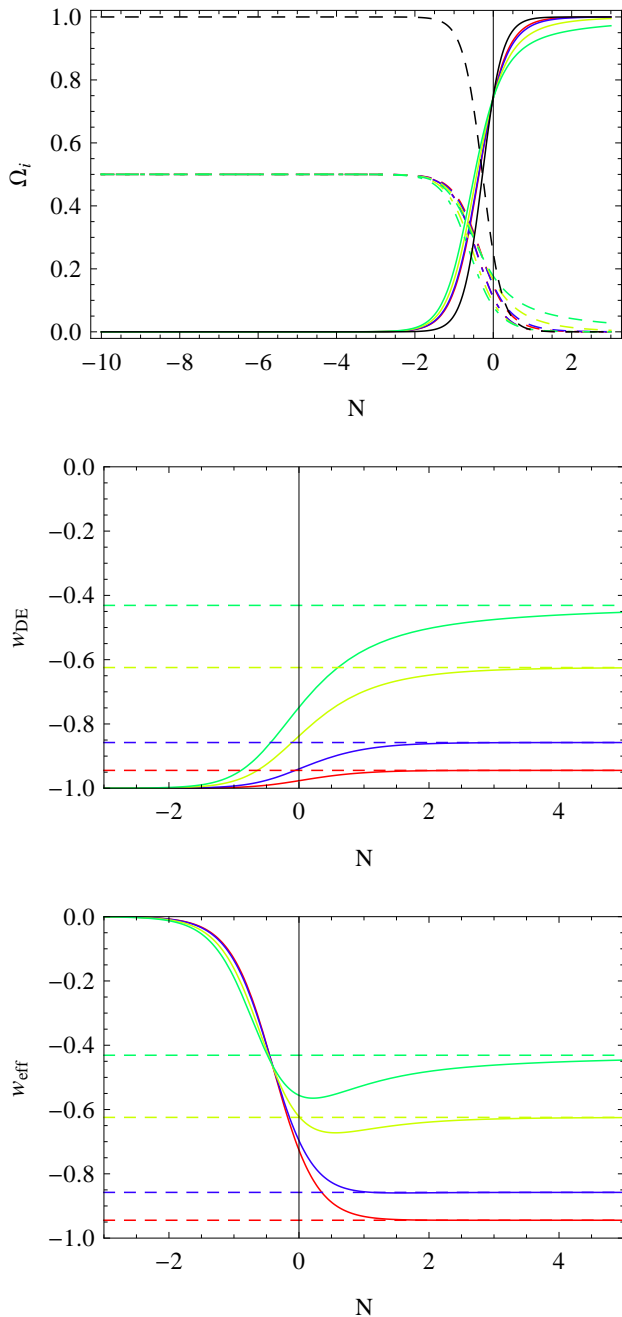


Figure 1: In the top panel we show plots of  $\Omega_{DE}$ ,  $\Omega_-$  (dot-dashed curve) and  $\Omega_+$  (dashed curve) for the case of coupling  $\beta = 1$  and  $\mu_{in} = 0$ , when (from bottom up)  $\alpha = 0.5$  (red curve),  $\alpha = 0.8$  (blue curve),  $\alpha = 1.3$  (yellow curve) and  $\alpha = 1.6$  (green curve). These values of  $\alpha$  belong to the  $1\sigma$ ,  $2\sigma$ ,  $3\sigma$  and  $> 3\sigma$  regions of the last panel of Fig. 6, respectively. The black curves correspond to the  $\Lambda$ CDM model, where  $\Omega_\Lambda$  is the solid black curve and  $\Omega_m$  is the dashed black curve. The second and third panels show plots of  $w_{DE}$  and  $w_{eff}$  for the same parameters with the same color coding. The horizontal dashed curves in the latter two panels are the corresponding theoretical predictions for the asymptotic behavior, again with the same color coding. All plots are with respect to the e-folding time variable  $N \equiv \ln a$ , where  $a$  is the scale factor. See Section II for more details. Note that vertical lines represent the present time, which corresponds to  $N = 0$ .

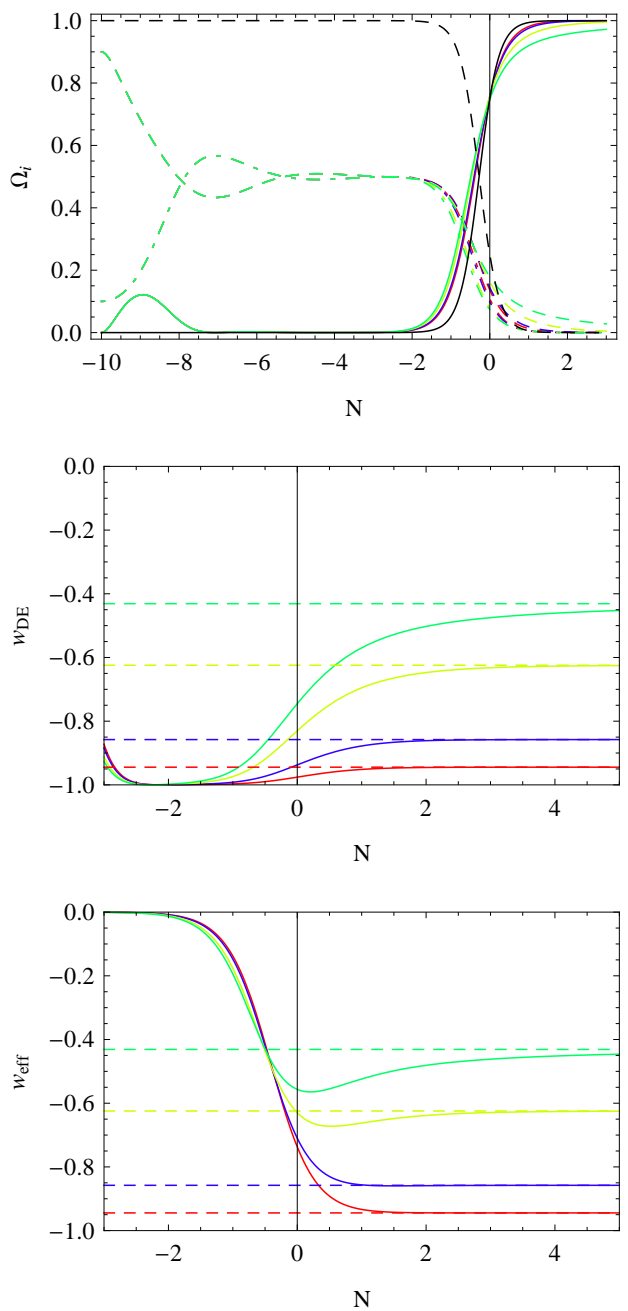


Figure 2: As in Fig. 1 but for  $\mu_{in} = 0.8$ .

Let us now introduce the following notation:

$$\frac{\dot{\phi}^2}{6M_{Pl}^2 H^2} = x^2, \quad (11)$$

$$\frac{V}{3M_{Pl}^2 H^2} = y^2, \quad (12)$$

$$\frac{\rho_\pm}{3M_{Pl}^2 H^2} = z_{1,2}^2, \quad (13)$$

$$\frac{\rho_r}{3M_{Pl}^2 H^2} = r^2, \quad (14)$$

After replacing the new variables (11-14) and introducing

the new e-folding time variable  $N \equiv \ln a$  (we will denote the derivative with respect to  $N$  with a prime) and after defining

$$\alpha = \sqrt{\frac{3}{2}} M_{Pl} \alpha_1, \quad (15)$$

we obtain the full set of phase-space equations of McDE cosmologies:

$$2 \frac{H'}{H} = -(3 - 3y^2 + 3x^2 + r^2), \quad (16)$$

$$x' = -x \frac{H'}{H} - 3x + \alpha y^2 + \beta(z_2^2 - z_1^2), \quad (17)$$

$$y' = -y \frac{H'}{H} - \alpha x y, \quad (18)$$

$$z_1' = -z_1 \frac{H'}{H} - \frac{3}{2} z_1 + \beta x z_1, \quad (19)$$

$$z_2' = -z_2 \frac{H'}{H} - \frac{3}{2} z_2 - \beta x z_2, \quad (20)$$

$$r' = -r \frac{H'}{H} - 2r. \quad (21)$$

The former system of field equations (2)-(6) are symmetric for opposite signs of  $y$ ,  $z_1$ ,  $z_2$  and  $r$ . However, only the square of these quantities has physical meaning and there is no need to consider solutions of both signs. Notice that the dark energy density is

$$\Omega_{DE} = x^2 + y^2 \quad (22)$$

and that

$$x^2 + y^2 + z_1^2 + z_2^2 + r^2 = 1, \quad (23)$$

so one variable is effectively superfluous. The dark energy equation of state and effective equation of state read respectively:

$$w_{DE} = \frac{x^2 - y^2}{x^2 + y^2}, \quad (24)$$

$$w_{\text{eff}} = x^2 - y^2. \quad (25)$$

We plot in Figs. 1 and 2 the behavior of the model for some selected values of the parameters. The top panels display plots of  $\Omega_{DE}$ ,  $\Omega_-$  and  $\Omega_+$  for  $\alpha = 0.5, 0.8, 1.3, 1.6$  and  $\beta = 1$ . These values are chosen to lie progressively farther from the SN best fit. Hence, as expected, we see that the plots deviate more and more from  $\Lambda$ CDM. The middle and bottom panels display the evolution of the dark energy equation of state (EOS)  $w_{DE}$  and effective EOS  $w_{\text{eff}}$ , respectively, for the same parameter values. For  $w_{DE}$  and  $w_{\text{eff}}$ , we also plot the theoretical predictions for the asymptotic behavior (see Section III). Notice that after an initial transient, the plots become insensitive to  $\mu_{\text{in}}$ , as will be confirmed quantitatively with the likelihood analysis of Section V.

### III. CRITICAL POINTS

The goal of this paper is the solution of the system of field equations (16)-(21) and the comparison with SN Ia data. Expressing  $z_2$  in terms of  $x, y, z_1$  via Eq. (23) and employing the fact that we are studying the background evolution in the matter era (and so  $r = 0$ ), we can reduce the system of equations by two. An important step is the analysis of the critical points  $x' = y' = z_1' = 0$ , i.e. the solution of the following system of equations:

$$0 = \frac{x}{2}(3 - 3y^2 + 3x^2) - 3x + \alpha y^2 \quad (26)$$

$$+ \beta(1 - x^2 - y^2 - 2z_1^2),$$

$$0 = \frac{y}{2}(3 - 3y^2 + 3x^2) - \alpha x y, \quad (27)$$

$$0 = \frac{z_1}{2}(3 - 3y^2 + 3x^2) - \frac{3}{2} z_1 + \beta x z_1. \quad (28)$$

We need to select the critical points which are real and physical, i.e. with real positive energy density less than unit. This implies  $|x| \leq 1$  and  $0 \leq y, z_1, z_2 \leq 1$ . Employing the symmetries under  $\beta \rightarrow -\beta$ ,  $z_1 \rightarrow z_2$ , and under  $\alpha \rightarrow -\alpha$ ,  $x \rightarrow -x$  and  $\beta \rightarrow -\beta$ , we can discard a number of symmetrical points and restrict our analysis to  $\alpha \geq 0$ ,  $\beta \geq 0$ ,  $\mu \geq 0$ . All the surviving points are listed in Table I. Since we need to have a final state that is accelerated ( $w_{\text{eff}} < -1/3$ ), only points 2 and 5 can be acceptable final states. The stable acceleration regions of points 2 and 5 are then found by linearly perturbing the system around these points.

The eigenvalues of the linearization matrix around point 2 are:

$$\begin{aligned} \lambda_1^{p2} &= \frac{-9 + \alpha^2}{3}, \\ \lambda_2^{p2} &= \frac{-9 + 2\alpha^2 - 2\alpha\beta}{3}, \\ \lambda_3^{p2} &= \frac{-9 + 2\alpha^2 + 2\alpha\beta}{6}, \end{aligned} \quad (29)$$

and its region of stability is defined by the condition  $\text{Re}[\lambda_{1,2,3}] < 0$ . The region of the parameter space that is stable and accelerated is shown in dark blue in Fig. 3. We will restrict the analysis of Sections IV and V to this region.

The eigenvalues for point 5 are:

$$\begin{aligned} \lambda_1^{p5} &= -\frac{6\beta}{\alpha + \beta}, \\ \lambda_2^{p5} &= -\frac{3\alpha + 6\beta + \Delta(\beta)}{4(\alpha + \beta)}, \\ \lambda_3^{p5} &= \frac{-3\alpha - 6\beta + \Delta(\beta)}{4(\alpha + \beta)}, \end{aligned} \quad (30)$$

where  $\Delta(\beta) \equiv [9(-36 + 7\alpha^2) + 4\alpha(-27 + 8\alpha^2)\beta + 4(-45 + 16\alpha^2)\beta^2 + 32\alpha\beta^3]^{1/2}$ . The region of stable acceleration for point 5 is shown in dark red in Fig. 3.

No	$x$	$y$	$z_1$	$z_2$	$\Omega_{\text{DE}}$	$w_\phi$	$w_{\text{eff}}$	$\mu$
1	$\pm 1$	0	0	0	1	1	1	0
2	$\frac{\alpha}{3}$	$\frac{1}{3}\sqrt{9-\alpha^2}$	0	0	1	$-1 + \frac{2\alpha^2}{9}$	$-1 + \frac{2\alpha^2}{9}$	0
3	0	0	$\frac{1}{\sqrt{2}}$	$\frac{1}{\sqrt{2}}$	0	0	0	0
4	$-\frac{2\beta}{3}$	0	$\sqrt{1 - \frac{4\beta^2}{9}}$	0	$\frac{4\beta^2}{9}$	1	$4\frac{\beta^2}{9}$	1
5	$\frac{3}{2(\alpha+\beta)}$	$\frac{\sqrt{9+4\alpha\beta+4\beta^2}}{2 \alpha+\beta }$	$\frac{\sqrt{-9+2\alpha\beta+2\alpha^2}}{\sqrt{2} \alpha+\beta }$	0	$\frac{9+2\alpha\beta+2\beta^2}{2(\alpha+\beta)^2}$	$\frac{-2(\alpha+\beta)\beta}{9+2\alpha\beta+2\beta^2}$	$\frac{-\beta}{(\alpha+\beta)}$	1

Table I: Critical points. Only points 2 and 5 can have accelerated expansion ( $w_{\text{eff}} < -1/3$ ). See Section III for more details.

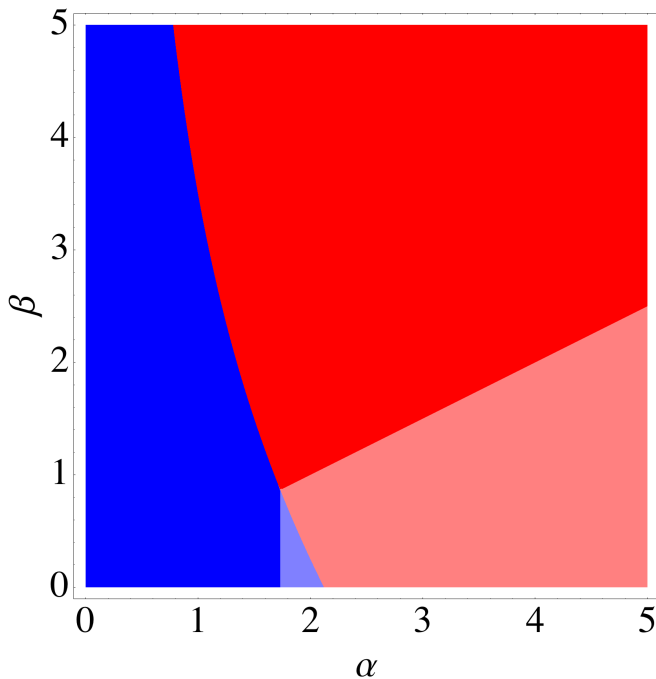


Figure 3: Regions of stability for point 2 (blue) and point 5 (red) of Table I. The darker blue and red regions have a final state that is accelerated ( $w_{\text{eff}} < -1/3$ ). In the following, we will restrict to these regions of stable acceleration.

Point 5 allows for a non-vanishing asymptotic value of  $\Omega_\pm$ , while still producing acceleration. This is illustrated in Fig. 4. Point 5 is interesting since it automatically selects one of the two forms of matter to dominate asymptotically along with dark energy, while the other one vanishes. This type of solutions, dubbed scaling or stationary solutions (see e.g. [5]), have been found in many other systems of interacting models.

#### IV. SN IA DATA AND METHOD

In order to constrain the parameters of the model discussed so far, we will use the Union2.1 Compilation [34] of

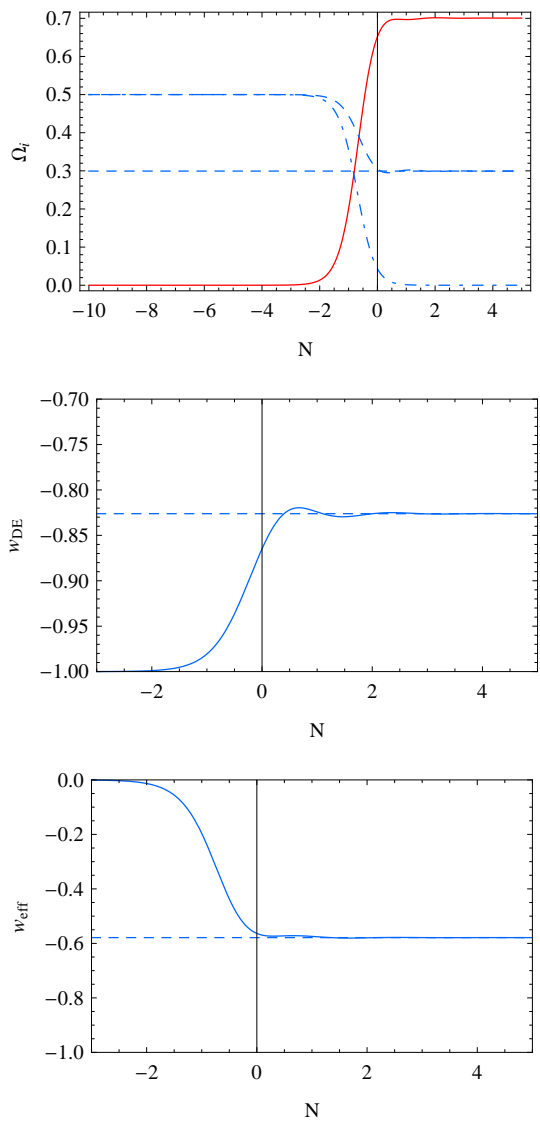


Figure 4: In the top panel,  $\Omega_{\text{DE}}$  (solid, red),  $\Omega_-$  (dot-dashed) and  $\Omega_+$  (dashed) for  $\beta = 3.52$ ,  $\alpha = 2.56$  and  $\mu_{\text{in}} = 0$ . For these values, point 5 is stable and accelerated. The second and the third panels show  $w_{\text{DE}}$  and  $w_{\text{eff}}$ , respectively. The long-dashed straight lines mark the asymptotic behaviors of the corresponding quantities. Plots are with respect to the e-folding time variable  $N$ .

580 Type Ia SN in the redshift range  $z = 0.015 - 1.414$ .<sup>1</sup> The predicted magnitudes are related to the luminosity distance  $d_L$  by:

$$m(z) = 5 \log_{10} \frac{d_L(z)}{10 \text{ pc}}, \quad (31)$$

which is computed assuming spatial flatness:

$$d_L(z) = (1+z) \int_0^z \frac{d\bar{z}}{H(\bar{z})}. \quad (32)$$

The likelihood analysis is based on the  $\chi^2$  function:

$$\chi_{SN Ia}^{\prime 2} = \sum_i \frac{[m_i - m(z_i) + \xi]^2}{\sigma_i^2}, \quad (33)$$

where the index  $i$  labels the elements of the Union2.1 dataset. The parameter  $\xi$  is an unknown offset sum of the supernova absolute magnitudes, of  $k$ -corrections and other possible systematics. As usual, we marginalize the likelihood  $L'_{SN Ia} = \exp(-\chi_{SN Ia}^{\prime 2}/2)$  over  $\xi$ ,  $L_{SN Ia} = \int d\xi L'_{SN Ia}$ , leading to a new marginalized  $\chi^2$  function:

$$\chi_{SN Ia}^2 = S_2 - \frac{S_1^2}{S_0}, \quad (34)$$

where we neglected a cosmology-independent normalizing constant, and the auxiliary quantities  $S_n$  are defined as:

$$S_n \equiv \sum_i \frac{[m_i - m(z_i)]^n}{\sigma_i^2}. \quad (35)$$

As  $\xi$  is degenerate with  $\log_{10} H_0$ , we are effectively marginalizing also over the Hubble constant.

The luminosity distance  $d_L(z)$  is obtained by integrating numerically Eqs (16)-(21). For every value of the parameters  $\alpha, \beta, \mu_{in}$  and every possible value of  $\Omega_{DE,0}$  we begin with a trial initial condition at a very large initial  $z$  that is given by  $\Lambda$ CDM with that particular  $\Omega_{DE,0}$  and with  $\Omega_{m,0} = \Omega_{+0} + \Omega_{-0} = 1 - \Omega_{DE,0}$ . At  $z = 0$  this solution will produce a  $\Omega_{DE,0}$  different from the  $\Lambda$ CDM value. We then perturb by trial and error the initial values of  $x, y, z_1, z_2$  until we find the sought-for  $\Omega_{DE,0}$ . We always impose as initial value  $x = 0$ .

## V. RESULTS

We will now show how the Union2.1 SN Compilation constrains the McDE scenario discussed in this paper. As discussed in Section III, we will consider only positive values of  $\{\alpha, \beta, \mu_{in}\}$  because of symmetry. Furthermore,

we will analyze separately the regions of stable acceleration of points 2 and 5 (dark blue and red in Fig. 3, respectively). The reason is that the attractor of point 2 depends only on  $\alpha$ , while the attractor of point 5 depends on both  $\alpha$  and  $\beta$ , as shown in Table I. Because of this degeneracy between  $\alpha$  and  $\beta$ , it is more instructive to keep the analysis of point 5 separate from the one of point 2.

### A. Constraints for critical point 2

Parameter	Best fit	95% c.l.
$\Omega_{DE,0}$	0.719	[0.680, 0.765]
$\alpha$	0.62	[0, 1.01]
$\beta$	6.4	[0, 83]
$\mu_{in}$	unconstrained	unconstrained

Table II: Best-fit values with 95% confidence intervals for the parameters of the model discussed in this paper. We employed a flat prior on the parameters, and in particular  $0 \leq \beta \leq 100$  and we explore here only the point 2 region of stability and acceleration. See Fig. 5 for a plot of the marginalized posterior distributions.

In order to constrain point 2 with the Union2.1 SN Compilation we compute the likelihood  $L_{SN Ia}$ , discussed in the previous Section, on a grid in the 4-dimensional parameter space  $\{\Omega_{DE,0}, \alpha, \beta, \mu_{in}\}$  and we marginalize analytically over the absolute magnitude of the supernovae.

Fig. 5 shows the marginalized posterior distributions on the single parameters. The best-fit values with 95% confidence levels are shown in Table II. From these results, it is clear that SNIa can constrain to a finite range both the present-day amount of dark energy  $\Omega_{DE,0}$  and the exponent  $\alpha$  of the potential. However, background observables such as SNIa can only marginally constrain the coupling  $\beta$  (the likelihood stays constant for values  $\beta > 100$ ) and cannot constrain at all the value of the asymmetry parameter  $\mu_{in}$ . In the top-left panel of Fig. 5 we also show the posterior of  $\Omega_{DE,0}$  for the case of the flat  $\Lambda$ CDM model (dotted curve). As one can see, the constraints are only slightly weaker for larger values of the dark energy density. Furthermore, the minimum  $\chi^2$  for the two models – McDE and  $\Lambda$ CDM – is approximately the same,  $\chi_{min}^2 = 562.2$ .

By comparing the best-fit values reported in Table II with the maximum of the posteriors shown in Fig. 5, one can notice a mismatch. To investigate this issue – and also the level of degeneracy between the parameters – we show in Fig. 6 the relevant 2-dimensional marginalized posterior distributions. One can see, perhaps a little surprisingly, that values of  $\Omega_{DE,0} \simeq 0.90$  are allowed at the  $3\sigma$  level; this is clearly due to the degeneracy between  $\Omega_{DE,0}$  and the parameter  $\alpha$  when  $\beta$  is negligible and it is similar to the well-known degeneracy between  $\Omega_{DE,0}$

<sup>1</sup> More precisely, we use the magnitude vs. redshift table publicly available at the Supernova Cosmology Project [webpage](#). This table does not include systematic errors.

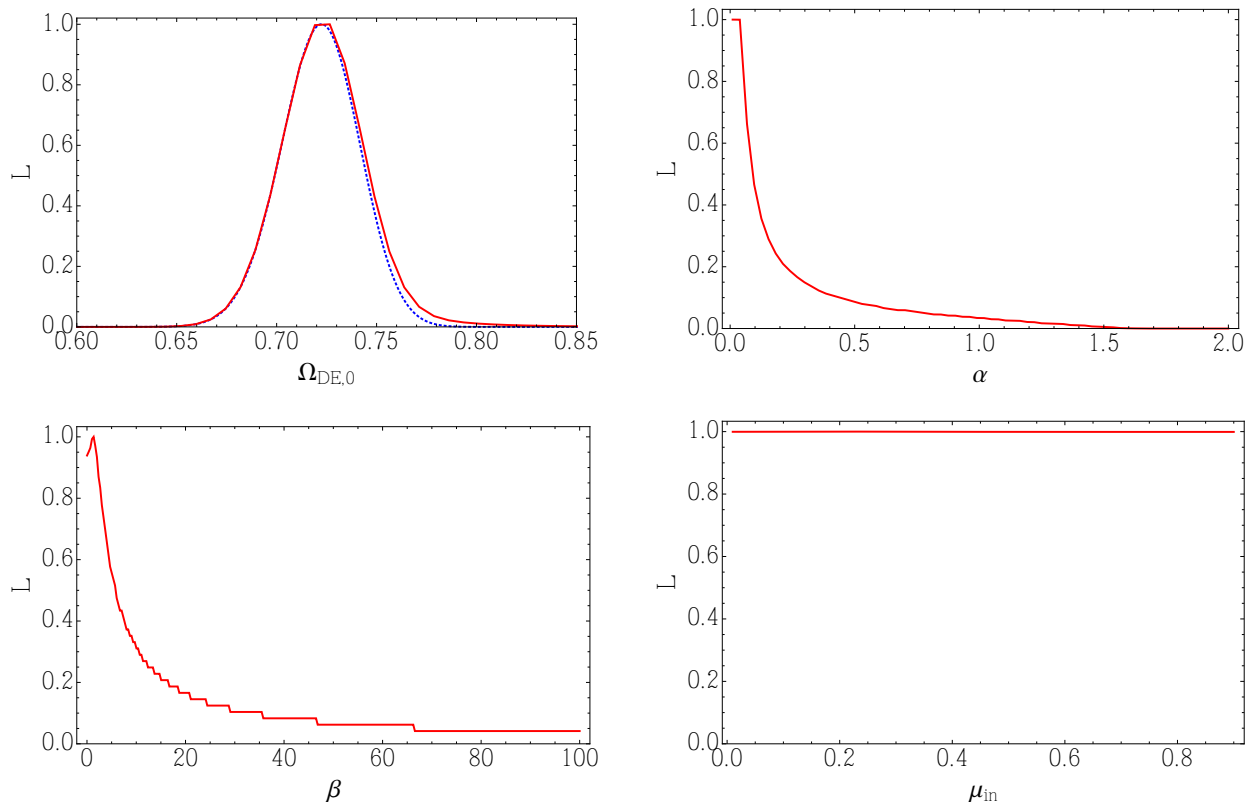


Figure 5: Marginalized posterior distributions for point 2 on the parameters  $\{\Omega_{\text{DE},0}, \alpha, \beta, \mu_{\text{in}}\}$  when fitting the model of this paper to the Union2.1 SN Compilation [34]. In the top-left panel the dotted curve is the posterior of the flat  $\Lambda$ CDM model. While SNIa observations constrain to a finite range of values both the present-day amount of dark energy  $\Omega_{\text{DE},0}$  and potential slope  $\alpha$ , they can only marginally constrain the coupling  $\beta$  and not at all the value of the asymmetry parameter  $\mu_{\text{in}}$ . See Table II for best-fit values with 95% confidence intervals.

and  $w$  for a dark energy model with constant EOS. Also, the posterior on  $\alpha$  and  $\beta$  shows a nontrivial likelihood surface. This explains the mismatch between the best-fit values of Table II and the maximum of the posterior on  $\alpha$ .

### B. Constraints for critical point 5

As anticipated and shown in Table I, the attractor of critical point 5 depends on both the potential slope  $\alpha$  and the coupling  $\beta$ . Therefore, a strong degeneracy between  $\alpha, \beta$  is to be expected. So as to better understand the behaviors of the solutions relative to point 5, we will then restrict to trajectories for which the asymptotic attractor has already been reached at the present time. If on one hand this simplifies and clarifies the analysis, on the other hand this choice worsens the overall fit ( $\chi_{\text{min}}^2 = 568.2$ ). This is to be expected as the effective EOS  $w_{\text{eff}}$  is now constant, and so clearly in tension with SN data. We checked that non-asymptotic solutions relative to point 5 can give as good a fit ( $\chi_{\text{min}}^2 = 562.4$ ) as point 2 and the flat  $\Lambda$ CDM model.

Fig. 7 shows the constraints from SNIa observations for the case of asymptotic solutions of point 5 for three

pairs of parameters. The top panel shows that values of the (constant) effective EOS  $w_{\text{eff}}$  quite larger than  $-1$  are preferred. This is to be expected as SNIa prefer models with  $w_{\text{eff}}$  evolving from 0 to  $\sim -1$  in the future, with a present value around  $w_{\text{eff}} \approx w\Omega_{\text{DE},0} \approx -\Omega_{\text{DE},0}$ . The second plot shows a nontrivial degeneracy between  $\Omega_{\text{DE},0}$  and  $\beta$ , while the bottom plot shows the expected very strong degeneracy between  $\alpha$  and  $\beta$ . From Table I one can in fact see that for large  $\alpha, \beta$  point 5 depends only on  $\beta/\alpha$ . The best-fit values for the three analyses are  $(\Omega_{\text{DE}}, w_{\text{eff}}) = (0.66, -0.57)$ ,  $(\Omega_{\text{DE}}, \beta) = (0.67, 3.82)$ ,  $(\alpha, \beta) = (2.56, 3.52)$ , respectively.

Summarizing, we found that the proposed model is compatible with SNIa observations in a large range of parameters. In particular, we find that the cosmic expansion is very weakly dependent on the dimensionless coupling constant  $\beta$  and even values of  $\sim 100$  (i.e. three orders of magnitude larger than present bounds on the coupling  $\beta \lesssim 0.1$  for standard cDE models) are allowed. Moreover, we found that the luminosity distance probed by SNIa data is insensitive to  $\mu_{\text{in}}$ . We have repeated the analysis of this Section using the forecasted Dark Energy Survey (DES) sample of 3000 SNe [14] and found that while the constraints on  $\Omega_{\text{DE}}$  become tighter, the

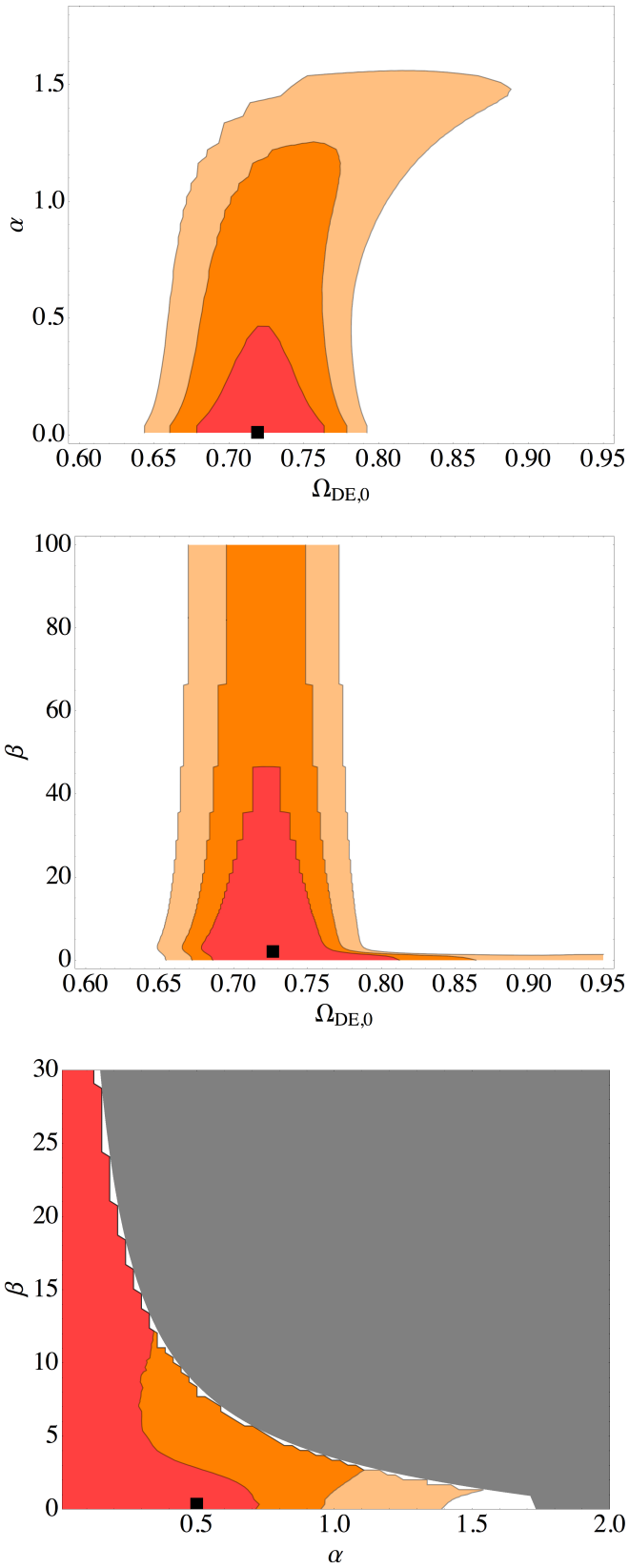


Figure 6:  $1\sigma$ ,  $2\sigma$  and  $3\sigma$  confidence-level contours for the relevant 2-dimensional marginalized posterior distributions for point 2. The black squares mark the best-fit values. The degeneracy between  $\Omega_{\text{DE},0}$  and the parameters  $\alpha, \beta$  makes values of  $\Omega_{\text{DE},0} \simeq 0.90$  possible at the  $3\sigma$  level. The bottom panel explains why the best fit has  $\alpha = 0.62$ , while the posterior on  $\alpha$  is peaked at  $\alpha = 0$ . The gray region is excluded, see Fig. 3.

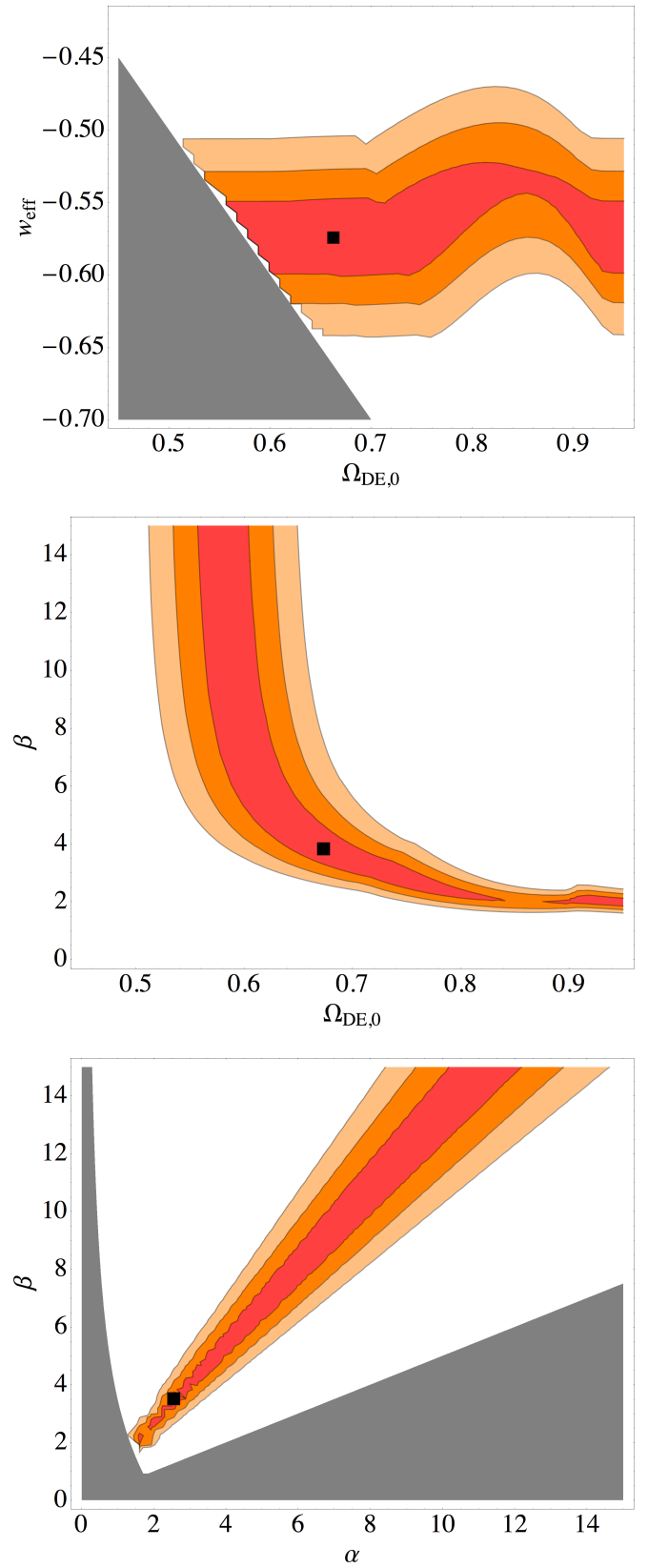


Figure 7:  $1\sigma$ ,  $2\sigma$  and  $3\sigma$  confidence-level contours for the 2-dimensional marginalized posterior distributions relative to asymptotic solutions of point 5. The black squares mark the best-fit values. The gray regions are excluded, see Fig. 3 and Table I. For each posterior, a flat prior on the parameters displayed in the plot has been adopted. Particularly evident is the degeneracy between  $\alpha$  and  $\beta$ .

constraints on the the McDE parameters  $\alpha, \beta$  are only marginally improved. This further demonstrates the ability of McDE to satisfy background observations.

We expect, however, that the value of  $\mu_{\text{in}}$  will be very important as far as structure formation is concerned and that the analysis of perturbations will bring improved constraints. In fact, as shown in [9], the perturbation equations of McDE cosmologies are unstable with respect to the asymmetry between the two different CDM species, due to the opposite signs of the extra-friction terms [see 9, for a more detailed discussion on the instability of adiabatic perturbations in McDE models]. As a consequence, the growing asymmetry at low redshifts related to the dynamical evolution of the background is expected to amplify the effects of the attractive and repulsive fifth-forces at the level of linear and nonlinear density perturbations [see again 10].

## VI. CONCLUSIONS

In the present paper, we have compared for the first time the Multi-coupled Dark Energy scenario proposed by [9] with observational data on the cosmic expansion history, consisting of the 580 Type Ia supernovae of the Union2.1 sample [34].

As a first step, we have performed a full analytic study of the dynamical system associated to the background equations of Multi-coupled Dark Energy, identifying the critical points of the system and investigating in full detail their existence and stability conditions. Among the physically consistent points, we have selected those giving cosmologically viable solutions. Such analysis has shown that all critical points are characterized by only three possible asymptotic values of the asymmetry parameter  $\mu$  that quantifies the relative abundance of the two CDM particle species. Such values are 0 and  $\pm 1$  (due to symmetry between  $\mu \rightarrow -\mu$ ), corresponding to a perfect balance between the two species and to the full domination of one of the two species over the other, respectively. This means that, independently of the initial value of the asymmetry parameter  $\mu$ , the asymptotic fate of the universe in McDE cosmologies will be characterized by either perfect symmetry between the two CDM species, or by the disappearance of one of the two. Additionally, our results identified a nontrivial solution for the future evolution of the universe characterized by a scaling between the Dark Energy and CDM relative densities that keep a constant ratio in the asymptotic future.

As a second step, we have performed a full likelihood analysis in the model's parameter space, restricting the

range of parameters based on the stability conditions previously obtained. As expected, we find that supernova data can constrain the slope of the self-interaction potential  $\alpha$ , which is found to be bound to values  $\lesssim 1.5$  at the  $3\sigma$  confidence level. On the other hand, we find a flat posterior likelihood for the initial asymmetry parameter,  $\mu_{\text{in}}$ , which is therefore completely unconstrained by the data, and more interestingly we derive the 1, 2, and  $3\sigma$  confidence regions in the parameter plane  $\beta - \Omega_{\text{DE},0}$ , showing very weak constraints on the coupling parameter  $\beta$ . In fact, couplings of the order of  $\beta \sim 10^2$  appear to be consistent at the  $2\sigma$  confidence level with the fiducial value of the Dark Energy fractional density. The correction to the gravitational force is proportional to  $\beta^2$ ; this implies that an extra force, four orders of magnitude stronger than gravity, would still go unnoticed in a SN Hubble diagram.

The results of our direct comparison show that the Multi-coupled Dark Energy scenario is practically indistinguishable from a standard  $\Lambda$ CDM cosmology at the background level, thereby providing a direct example of how the background expansion history might be almost insensitive to the internal complexity of the dark sector. These conclusions still hold if one uses the forecasted DES sample of 3000 SNIa instead of the Union2.1 SN Compilation.

Observational constraints on the linear growth of density perturbations, and ultimately the detailed investigation of the impact of Multi-coupled Dark Energy models on the dynamical evolution of nonlinear structures at small scales, promise to place much tighter bounds on the model's parameter space, and will be investigated in future works. For now, our investigation demonstrates the full viability of Multi-coupled Dark Energy as an alternative to the  $\Lambda$ CDM cosmology for what concerns the cosmic expansion history.

## Acknowledgments

A.P. is grateful for the hospitality of the ITP, University of Heidelberg, where most of this work was prepared. A.P. acknowledges funding by DAAD for financial support. M.B. is supported by the Marie Curie Intra European Fellowship "SIDUN" within the 7th Framework Programme of the European Community and also acknowledges partial support by the DFG Cluster of Excellence "Origin and Structure of the Universe". L.A., M.B. and V.M. acknowledge partial support from the TRR33 Transregio Collaborative Research Network "The Dark Universe".

---

[1] Aarssen L. G. d., Bringmann T., Pfrommer C., 2012, arXiv:1205.5809

[2] Ade P., et al., 2013, arXiv:1303.5076

[3] Amendola L., 2000, Phys. Rev., D62, 043511

- [4] Amendola L., Baldi M., Wetterich C., 2008, *Phys. Rev. D*, 78, 2, 023015
- [5] Amendola L., Quartin M., Tsujikawa S., Waga I., 2006, *Phys. Rev. D*, 74, 2, 023525
- [6] Amendola L., Tsujikawa S., 2010, *Dark Energy: Theory and Observations*, Cambridge University Press
- [7] Armendariz-Picon C., Mukhanov V. F., Steinhardt P. J., 2001, *Phys. Rev.*, D63, 103510
- [8] Baldi M., 2011, *MNRAS*, 411, 1077
- [9] Baldi M., 2012, *Annalen der Physik*, 524, 602
- [10] Baldi M., 2012, arXiv:1206.2348
- [11] Baldi M., Pettorino V., Robbers G., Springel V., 2010, *MNRAS*, 403, 1684
- [12] Batista R., Pace F., 2013, arXiv:1303.0414
- [13] Bean R., Flanagan E. E., Laszlo I., Trodden M., 2008, *Phys. Rev.*, D78, 123514
- [14] Bernstein J., Kessler R., Kuhlmann S., Biswas R., Kovacs E., et al., 2012, *Astrophys.J.*, 753, 152
- [15] Bode P., Ostriker J. P., Turok N., 2001, *Astrophys. J.*, 556, 93
- [16] Brookfield A. W., van de Bruck C., Hall L. M. H., 2008, *Phys. Rev.*, D77, 043006
- [17] Creminelli P., D'Amico G., Norena J., Senatore L., Vernizzi F., 2010, *JCAP*, 1003, 027
- [18] Creminelli P., D'Amico G., Norena J., Vernizzi F., 2009, *JCAP*, 0902, 018
- [19] Damour T., Gibbons G. W., Gundlach C., 1990, *Phys. Rev. Lett.*, 64, 123
- [20] Feng J. L., Kaplinghat M., Yu H.-B., 2010, *Phys. Rev. Lett.*, 104, 151301
- [21] Hu W., Sawicki I., 2007, *Phys. Rev.*, D76, 064004
- [22] Khlopov M. Y., 1995, 133–138
- [23] La Vacca G., Kristiansen J. R., Colombo L. P. L., Mainini R., Bonometto S. A., 2009, *JCAP*, 0904, 007
- [24] Li B., Barrow J. D., 2011, *Phys. Rev.*, D83, 024007
- [25] Loeb A., Weiner N., 2011, *Phys. Rev. Lett.*, 106, 171302
- [26] Macciò A. V., Quercellini C., Mainini R., Amendola L., Bonometto S. A., 2004, *Phys. Rev.*, D69, 123516
- [27] Maccio' A. V., Ruchayskiy O., Boyarsky A., Munoz-Cuartas J. C., 2012, arXiv:1202.2858
- [28] Medvedev M. V., 2013, arXiv:1305.1307
- [29] Pettorino V., Amendola L., Baccigalupi C., Quercellini C., 2012, *Phys.Rev.*, D86, 103507
- [30] Pettorino V., Amendola L., Wetterich C., 2013, arXiv:1301.5279
- [31] Ratra B., Peebles P. J. E., 1988, *Phys. Rev.*, D37, 3406
- [32] Salvatelli V., Marchini A., Lopez-Honorez L., Mena O., 2013, arXiv:1304.7119
- [33] Sefusatti E., Vernizzi F., 2011, *JCAP*, 1103, 047
- [34] Suzuki N., Rubin D., Lidman C., Aldering G., Amanullah R., et al., 2012, *Astrophys.J.*, 746, 85
- [35] Vogelsberger M., Zavala J., 2013, *MNRAS*
- [36] Wetterich C., 1988, *Nucl. Phys.*, B302, 668
- [37] Wetterich C., 1995, *Astron. Astrophys.*, 301, 321
- [38] Xia J.-Q., 2009, *Phys. Rev.*, D80, 103514